Nondestructive Raman Spectroscopy as a Tool for Early Detection and Discrimination of the Infection of Tomato Plants by Two Economically Important Viruses

Early detection and discrimination of two different viruses infecting tomato by non-destructive Raman spectroscopy

Luisa Mandrile[†], Silvia Rotunno[‡], Laura Miozzi[‡], Anna Maria Vaira[‡], Andrea M. Giovannozzi[†], Andrea M. Rossi[*†], Emanuela Noris[*‡]

[†]Istituto Nazionale di Ricerca Metrologica, Strada delle Cacce, 91 10135 Torino, Italy

[‡]Institute for Sustainable Plant Protection, National Research Council of Italy, Strada delle Cacce 73, 10135, Torino, Italy

Corresponding Authors

[*]E-mail: emanuela.noris@ipsp.cnr.it

[*]E-mail: a.rossi@inrim.it

Abstract

Global population forecasts dictate a rapid adoption of multifaceted approaches to fulfill increasing food requirements, ameliorate food dietary value and security using sustainable and economically feasible agricultural processes. Plant pathogens induce up to 25% losses in vegetable crops and their early detection would contribute to limit their spread and economic impact. As an alternative to time-consuming, destructive and expensive diagnostic procedures, such as immunological assays and nucleic acid-based techniques, Raman spectroscopy (RS) is a non-destructive rapid technique that generates a chemical fingerprinting of a sample at low operating costs. Here, we assessed the suitability of RS combined to chemometric analysis to monitor the infection of an important vegetable crop plant, tomato, by two dangerous and peculiarly different viral pathogens, *Tomato yellow leaf curl Sardinia virus* (TYLCSV) and *Tomato spotted wilt virus* (TSWV). Experimentally inoculated plants were monitored over 28 days for symptom occurrence and subjected to RS analysis, alongside with the evaluation of virus amount by quantitative real-time PCR. RS allowed to discriminate mock-inoculated (healthy) from virus-infected specimens reaching accuracy >70% after only 14 days after inoculation for TYLCSV and >85% only after 8 days for TSWV, demonstrating its suitability for early detection of virus infection. Importantly, RS highlighted also spectral differences induced by the two viruses, providing specific information on the infecting agent.

Keywords: Raman Spectroscopy; plant virus; biotic stress; precision agriculture; tomato; virus diagnosis

INTRODUCTION

Intelligent and sustainable agricultural practices represent an outstanding need in view of the world's population outreach of 9 billion of individuals within 2050 [1]. Vegetable crops are fundamental for the human diet and economically remunerative for the agricultural sector, but according to FAO estimates, transboundary plant pests provoke up to 25% of crop failures, entailing significant economic losses and contributing to food scarcity. Therefore, innovative strategies for disease prevention and for limiting pathogen spread are mandatory to reduce failures.

Tomato (*Solanum lycopersicum* L.) is the most economically important vegetable crop, with a total harvested area of 4.7 million ha, a production of 180 million tons (http://faostat3.fao.org/home/index.html) and a consumption exceeding 20 kg/person/year, with a still expanding trend [2]. Tomato suffers from attacks caused by >200 pests and diseases [2], currently controlled by chemical treatments, generating negative side effects such as pesticide resistance, environmental risks, and health issues for farmers and consumers. Among tomato pathogens, viruses play a significant role; two of them, *Tomato spotted wilt virus* (TSWV) and *Tomato yellow leaf curl virus* (TYLCV), are among the most ten destructive viruses of vegetables [3].

TSWV (Family *Tospoviridae*), with a tripartite single-stranded (ss) RNA genome [4], infects up to 900 plant species [5,6], causing over 1 billion $ losses worldwide [7,8]. On tomato, it induces inward cupping and drooping of leaves, unilateral plant growth, stunting and ultimately death; if present, fruits display chlorotic/necrotic ring spots and become unmarketable. TYLCV and its relative *Tomato yellow leaf curl Sardinia virus* (TYLCSV) belong to the *Geminiviridae* family, with a circular ssDNA genome encapsidated in geminated particles, causing huge economic losses on food and cash crops [9]. TYLCSV and TYLCV are responsible for the tomato leaf curl disease and are transmitted by whiteflies in a circulative persistent manner [10].

Early detection of plant pathogens is fundamental to prevent disease spread, limit crop damages and regulate proper pesticide use, under sustainable crop management practices. Identification of pathogens by visual assessment must be supported by objective and “non-operator dependent” diagnostic techniques. Immunological assays are commonly used for tospovirus diagnosis [11], while microarrays allows virus detection and species identification [12] and quantitative PCR (qPCR) is suitable for species identification and virus quantification [11,13]. For tomato leaf curl disease viruses, molecular hybridization and PCR are preferred diagnostic techniques [14,15], and qPCR allows absolute and relative quantifications [16,17]. Although these traditional assays are sensitive, accurate, and effective to confirm visual inspection, they are unsuitable for rapid large scale monitoring of plants before symptom onset, as they are destructive and require detailed sampling procedures, expensive infrastructures, and skilled personnel. Therefore, innovative, non-invasive, and non-

destructive methods for disease detection have been proposed, based on fluorescence, volatile sensors and imaging, but these are still at an experimental stage [18]. Spectroscopic techniques have interesting applications and, unlike other methods, are simple, rapid and affordable [18,19]. Among them, Raman spectroscopy (RS) has been applied in the biomedical sector to whole cells, tissues, and fluids [20]. In the agricultural fields, RS was considered for species-specific analysis for feed safety and traceability [21] and contaminant detection [22]. RS provides specific biochemical fingerprints reflecting detailed chemical and structural alterations [23], possibly representing sensitive and phenotypic markers of a disease. In plant pathology, RS was proposed to differentiate pepper plants infected by tobamoviruses [24] and *Abutilon* spp. plants infected by the geminivirus *Abutilon mosaic virus* [25], concluding that carotenoid content was a discriminatory variable. More recently, RS was also used for early diagnosis of a phytoplasma on sweet orange [26] and for fungal pathogen detection on maize kernels [27].

Here, we applied RS for the early and discriminative detection of two important viruses of tomato, in a dynamic infection time-frame. Tomato plants inoculated with TSWV and TYLCSV were visually inspected for symptoms for up to 28 days after inoculation, tested for relative viral accumulation by qPCR, and subjected to non-destructive RS analysis on leaves. Beside RS peaks assignment, a chemometric approach for data analysis was adopted to overcome the difficulties to interpret chemical information contained in the spectra of whole biological samples. Principal Components Analysis (PCA) [28] helped to determine systematic differences in the profiles of healthy and infected plants. Moreover, the sensitivity, precision and accuracy of RS to detect plant infection by partial least square-discriminant analysis (PLS-DA) were assessed, obtaining satisfactory classification rates starting from 8 days after inoculation for TWSV and from 14 days after inoculation for TYLCSV, time points at which viral symptoms were visually undetectable.

EXPERIMENTAL SECTION

Plant growth and treatments. Tomato plants (n = 3) grown in soil at 23 °C were inoculated with TYLCSV or with TSWV (see Supporting Information). Symptoms, relative virus amount, and RS were monitored weekly from 0 to 28 days post inoculation (dpi), using mock-inoculated plants as control. For TSWV, plants were also tested at 2, 5 and 8 dpi.

Nucleic acid (NA) extraction. NA were extracted from the basal leaflets of the second true leaf from the apex of each plant. For TYLCSV-infection, total DNA was extracted by the dot-blot method [16] and used for qPCR, while for TSWV, RNA was extracted with Trizol® and processed for qRT-PCR.

Quantitative Real-Time PCR for relative virus quantification. TYLCSV was quantified using tomato ascorbate peroxidase (APX) as housekeeping gene (Table S1), while the ubiquitin-conjugating enzyme (UBC) was used as housekeeping transcript for TSWV. Reactions were performed with iTaq™ Universal SYBR® Green Supermix (10-µl volume) and the CFX Connect™ Real-Time PCR Detection System (three technical replicates; see Supporting Information). The relative viral amount was calculated by the comparative threshold cycle (ΔC_t) method, where ΔC_t is $|C_{t\ virus} - C_{t\ housekeeping\ gene}|$.

Raman spectroscopic measurements. Three Raman spectra were acquired from the apical leaflets of the second leaf counting from the apex, immediately prior to sample collection for virus quantification. Leaves were stored in plastic bags at 4 °C until spectra acquisition, occurring within the following four hours. Spectra (400-3100 cm^{-1}; 5 cm^{-1} resolution) were obtained with a Dispersive Raman Spectrometer DRX (780 nm excitation laser, 10X microscope objective, 2 µm laser spot diameter, 2 mW laser power, 5 sec/15 scansions acquisition time). The spectrometer was weekly calibrated using a certified white light for intensity and neon gas lines for frequency. Moreover, a Si standard was measured before each session, to guarantee consistency within measurements and avoid differences due to instrument performances.

Chemometric analysis of Raman spectra. Chemometric analysis was conducted using the PLS Toolbox (Eigenvector Research, Inc., Manson, WA) for Matlab R2015a (Mathworks, Natick, MA). We used PCA to find correlations between measurements and the effect of virus infection and calculated PLS-DA models [29] to determine RS sensitivity for early virus infection. Models were cross-validated with the "leave-one group-out", using subsets of samples constituting the sets for cross-validation corresponding to one plant at a time. To compare classification performances at different plant ageing levels (0-28 dpi), we calculated Sensitivity [True Positive/(True Positive+False Negative)], Specificity [True Negative/(True Negative+False Positive)], Accuracy (correctly classified samples/total samples), and Classification Error (1-Accuracy). Spectra were pre-processed by Savitsky-Golay smoothing (31 points, polynomial order 2), removing Random shift of the baseline offset by weighted least squares baseline correction (polynomial order 2) [30]. Multiplicative scattering correction and mean centering were used. The same preprocessing was adopted for PCA and PLS-DA.

RESULTS AND DISCUSSION

Visual symptom and virus quantification. Viruses induce a variety of systemic symptoms on plants that increase with time progression depending on the pathogen, the plant species, the time of infection, and the environment. In our experimental conditions, TYLCSV symptoms consisting of

leaf yellowing and curling became evident at 28 dpi (Figure 1A), while for TSWV, chlorotic spots appeared on newly emerging leaves since 8 dpi (Figure 1B). qPCR showed that TYLCSV progressively increased from 7 to 28 dpi, following a logarithmic scale ($R^2 = 0.9984$, $P<0.001$) (Figure 1C). Instead, TWSV accumulated faster, as its steady-state level was reached at 5 dpi (Figure 1D), in line with the more precocious symptom onset. Noteworthy, TSWV amount remained stable up to 28 dpi (Figure 1D) while symptoms progressively deteriorated, indicating that cumulative effects due to cell metabolism perturbation [31] rather than virus accumulation could be responsible for symptom progression.

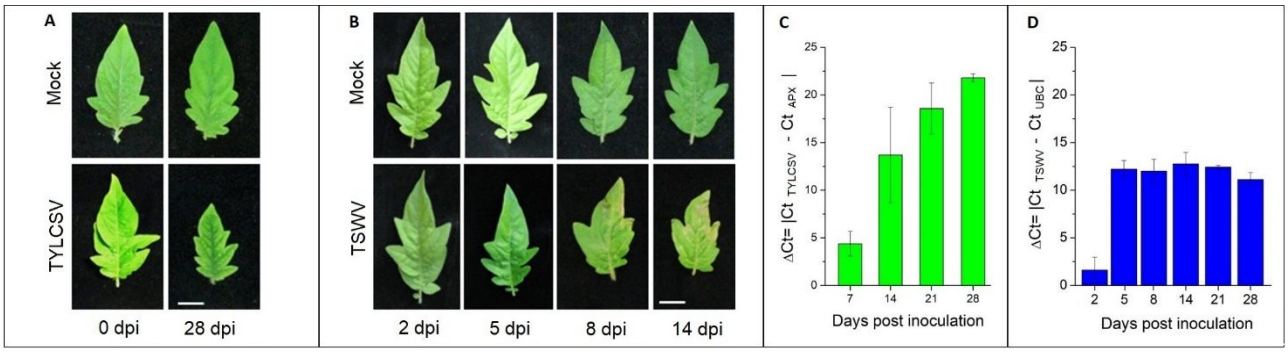

Figure 1. Infection of tomato plants by TYLCSV and TSWV. Images of leaflets collected before (0 dpi) and at different time points after inoculation with TYLCSV (A) or TSWV (B). Images of TSWV-infected leaves after 14 dpi are not shown, as they were clearly symptomatic. Bar = 1 cm. Relative accumulation of TYLCSV (C) and TSWV (D) in leaf tissue, at different times post-inoculation. Results are expressed as ΔC_t values, representing the difference between the threshold cycle (C_t) of each sample and that of the reference gene (APX for TYLCSV) or of the reference transcript (UBC for TSWV). Bars are the mean value of three plants, while vertical lines on each bar are the standard error.

Unsupervised data analysis of Raman spectra during virus infection. The vibrational bands obtained from the normalized average RS recorded on tomato leaves (Figure 2) were assigned to corresponding functional groups and biochemical species; the majority of peaks were attributed to carotenoids, chlorophyll and carbohydrates (Table 1). Specifically, carotenoids generated bands at 1526, 1153, and 1000 cm^{-1}, due to C=C and C–C stretching and to in-plane CH_3 rocking modes [32,33], as well as bands at 1387, 1328, and 1184 cm^{-1} [34,35]. The structure of carotenoids shows various CH_3 groups attached to C=C responsible for the band at 1387 cm^{-1}, but the band linked to this bending was relatively weak. Other bands associated with =CH rocking are visible at 1330-1250 cm^{-1}, whereas the band at 1184 cm^{-1} is again assigned to a C–C stretching mode. The weak bands at 1353, 1287 and 915 cm^{-1} and the shoulders at 1551 and 987 cm^{-1} associated to chlorophyll [36] partially overlapped with those of certain carotenoids around 1350-1280 cm^{-1} [33]. Other components identified in the spectra represented cellulose and hemicellulose, with limited contributions [37], and

lignin (characteristic peak at 1608 cm^{-1}; C-C stretching) [27]. The contribution of monomeric sugars and starch was observed at 1153 cm^{-1} and in the region 940-850 cm^{-1} (C-O-C vibration, typical of starch), while bands at 1110, 1070, 1047 and 1026 cm^{-1} are associated to C-OH, related to monomeric sugars.

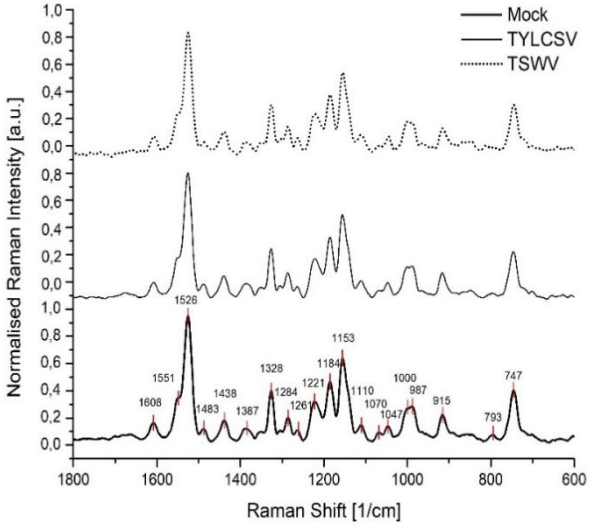

Figure 2. Mean Raman spectra of tomato leaves obtained from plants mock-inoculated (healthy) and infected by either TYLCV or TSWV. Spectra of all tested plants were averaged to obtain the three spectra shown.

Table 1. Vibrational bands and their assignments for tomato leaf samples.

Band	Vibrational assignment
1608	m ν(phenyl ring) (phenolics and lignin) [38]
1551	m br chlorophyll - central 16-membered-ring vib.+ ν(C=C) (pyrrole ring)
1526	s ν1(C-C) (carotenoids)[39]
1438	m ν(phenyl ring) (phenolics) [38]
1483	m δ(CH_2) and δ (CH_3)
1328	m δ(CH). ν(CN) (pyrrole ring br. - chlorophylls) [40]
1353	w undefined (chlorophylls)
1387	w δ(CH_3) (β-carotene and luteine)[25]
1284	m δ(phenyl-OH) (phenolics) [38] + - δ(CH). ν(CN) (chlorophyll)[25]
1261	w ro(=CH) (carotenoids)[25]
1222	m δ(CH). δ(CH_2) (chlorophyll)[40]
1125-1185	ms ν(CC). γ(CH) (chlorophylls)[40] + δ(CH phenyl) phenolics)[38]
1153	s ν2(C\\C) (carotenoids) [41]
1144	m sh ν(CN). δ(CNC) (chlorophyll)[40]

1110	δ (C-OH) (carbohydrates)[27]
1070	δ (C-OH) (carbohydrates)[27]
1047	ν (C-O)+ ν(C-C)+ ν(C-OH) (carbohydrates)[27]
1000	m δ(C-CH_3) (carotenoids)[41]
987	m undefined (chlorophylls)
915	m undefined (chlorophylls)
747	m-s ring br. Mode (aromatics)

m=medium w=weak ms= medium strong

Overall, the spectral profiles for healthy and for TYLCSV- or TSWV-infected plants showed similar patterns (Figure 2); in both cases, signals due to chlorophylls were remarkably weaker than those assigned to carotenoids and even weaker in infected plants, as previously described [25], providing a clear indication of metabolic changes occurring during infection [42].

Contrary to a recent RS analysis on plants subjected to abiotic stress [43], it was difficult to identify single Raman bands strongly altered by virus infection. Therefore, to straightforwardly interpret data and emphasize systematic spectral variations, a chemometric analysis was applied, a process that could be unnecessary for plants subjected to abiotic stresses, eliciting more uniform and synchronous metabolic responses in all cells, as opposed to the progressive changes on newly emerging tissue occurring during systemic pathogen infection.

At first, we investigated by PCA non-random variability associated with virus infection, obtaining a systematic grouping of spectra linked to the progression of both plant ageing and virus infection. To determine the effect of each virus, two separate PCA models were calculated. For TYLCSV, the most informative spectral regions within 950-1250 cm^{-1} and 1320-1640 cm^{-1} were considered (Figure 3).

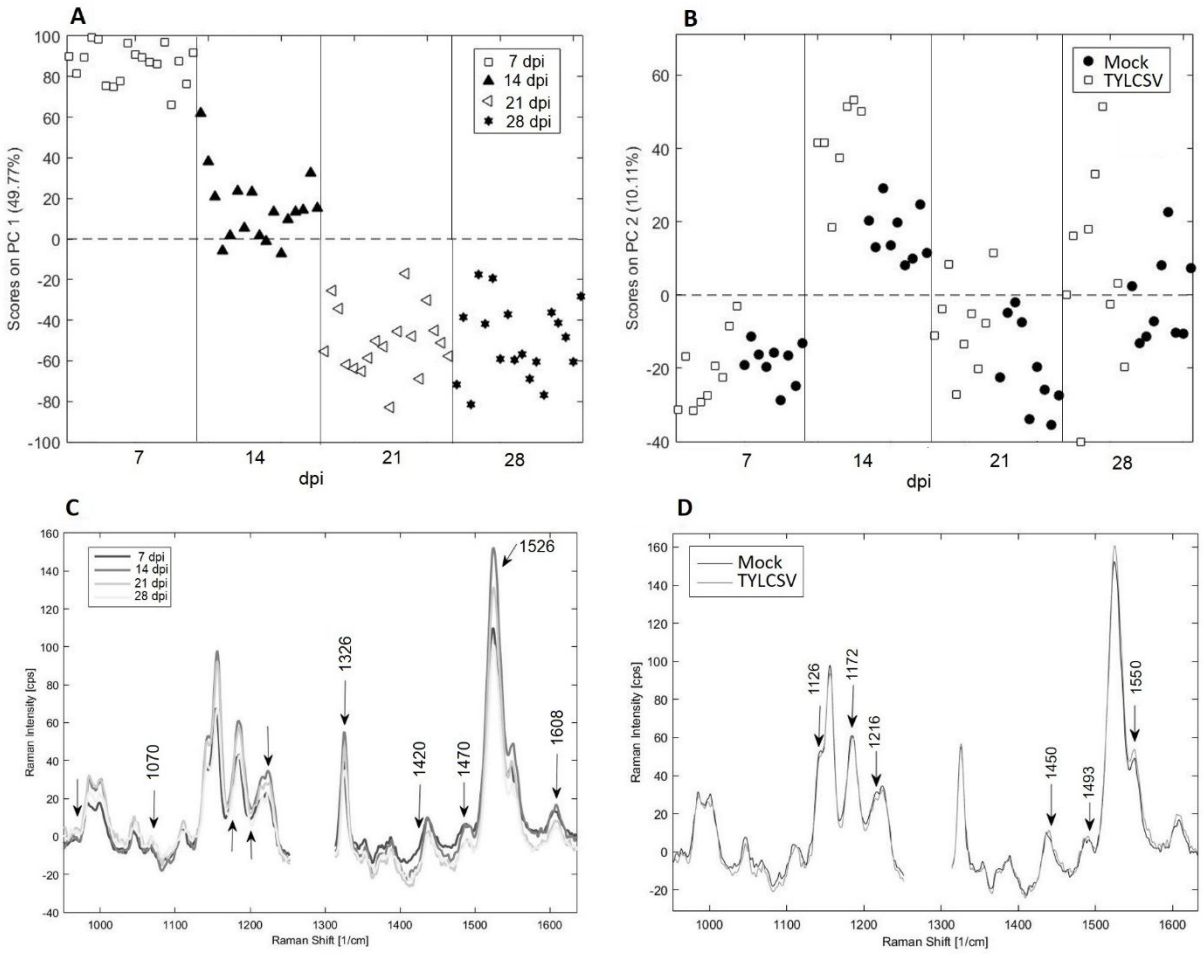

Figure 3: PCA model for TYLCSV-inoculation experiment. (A, B) PCA score plots as a function of time for the two first components. (C) Average tomato leaf spectra for each time point of analysis; arrows indicate the bands mainly represented in PC1, mostly correlated with time progression. (D) Average tomato leaf spectra of all mock-inoculated and all TYLCV-infected plants; arrows indicate bands mainly represented in PC2, mostly correlated with TYLCV infection.

The scores of the first two components plotted against time progression indicated significant differences among samples along the entire experimental period. In particular, PC1 mainly captured changes correlated with plant ageing, with scores progressively decreasing from 7 to 28 dpi (Figure 3A), while PC2 caught spectral modifications due to virus infection, as infected leaves showed scores lower than healthy ones, at the corresponding time points (Figure 3B). The loadings of the model and the histogram of the variance of spectral frequencies captured by each component (Figure S1) show the bands or the spectral regions responsible for sample grouping on the scores plot. Specifically, at 7 dpi (very early stage of infection), all signals displayed a relatively low intensity that increased at 14 dpi (early infection) and gradually decreased thereafter. However, the general intensity was not as informative as the differences in the intensity ratio and the shape of bands. The signals represented in PC1 (marked by arrows in Figure 3C) are mainly related to plant ageing and derive in particular from the carotenoid peak (1526 cm^{-1}) that underwent a slight

frequency shift and a bandwidth modification over time. A non-negligible contribution arose also from the 1470 cm^{-1} peak and the small shoulder at 1420 cm^{-1} that decreased from 7 to 28 dpi, together with the chlorophyll band at 1326 cm^{-1}. Other important contributions to PC1 arose also by the triplet bands between 1250-1100 cm^{-1}, again related to carotenoids and chlorophylls; on the contrary, an increase in the 1070 cm^{-1} peak (C-OH in carbohydrates) was recorded. In conclusion, the RS analysis of TYLCSV-infected plants identified a decrease in signals related to carotenoid/chlorophylls along with an increase in carbohydrates accumulation.

Interestingly, complementary bands represented in PC2 resulted more related to the virus presence (Figure 3D). Here, the peak shoulder at 1150 cm^{-1}, associated with the pyrrole ring stretching of chlorophylls, played a relevant role, together with the two smaller bands between 1500-1400 cm^{-1} related to phenolic compounds. PC2 also captured signals with significant variance at 1216, 1172 cm^{-1} and the shoulder at 1126 cm^{-1} probably due to chlorophylls. In conclusion, although single Raman bands affected by TYLCSV infection could not be identified, the entire spectral profile showed modifications in the regions associated to chlorophylls and phenolic compounds, at least in the period of infection considered. Interestingly, the early identification of a decrease in chlorophyll content in TYLCSV-infected plants is in line with the reported transcriptional perturbation of this metabolic pathway [44].

Similar experimental evidence was also recorded in the PCA model obtained for TSWV on spectra between 700 and 1800 cm^{-1} (Figure 4). In the long-term TSWV-infection analysis (7 to 28 dpi), both PC1 and PC2 resulted related to plant ageing and virus infection, contrary to the results with TYLCSV. In fact, TSWV -infected plants showed higher scores on PC1 at 21 and 28 dpi (Figure 4A) and, concurrently, the scores on PC2 of TSWV-infected plants were generally lower than control plants, at the corresponding time points (Figure 4B).

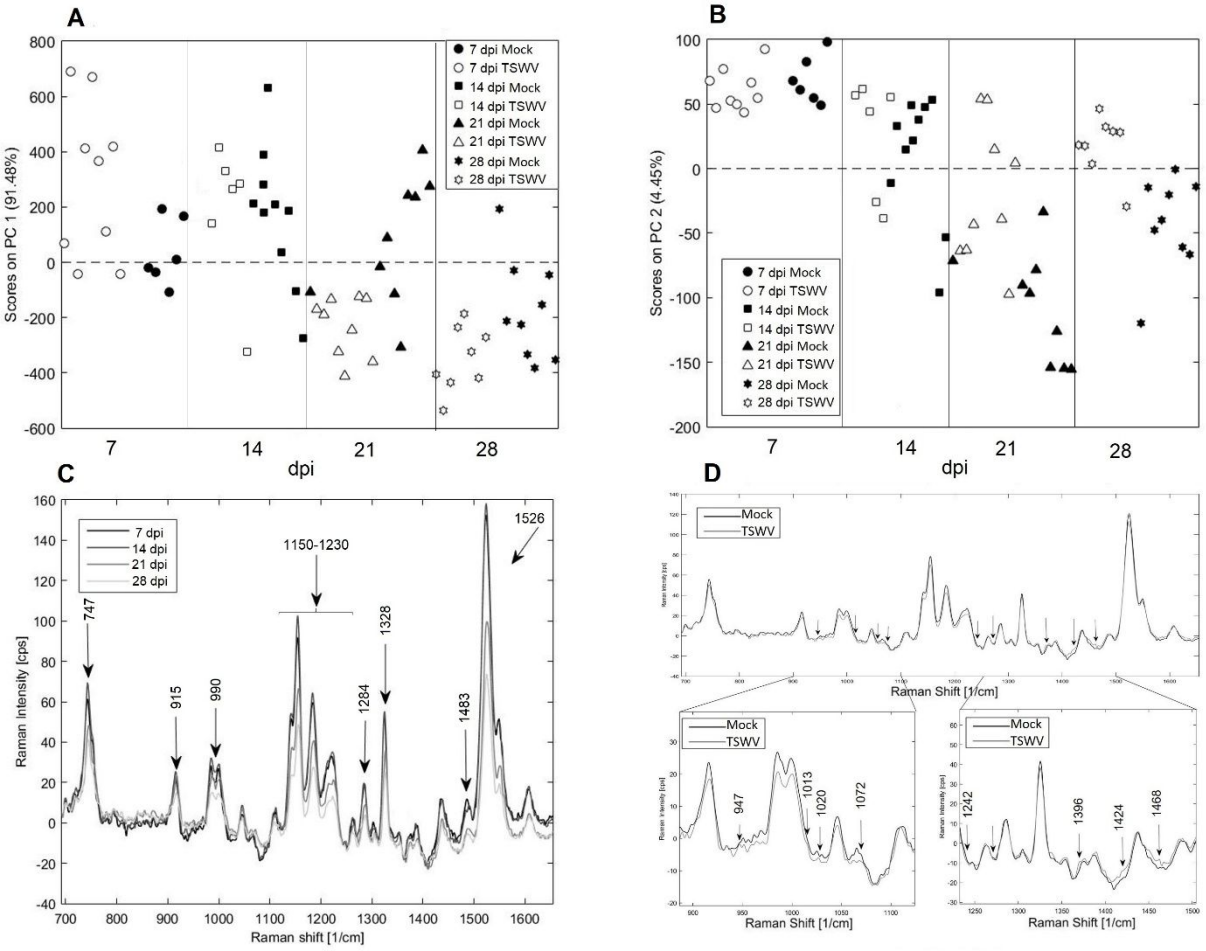

Figure 4: PCA model for TSWV inoculation experiment. (A) PCA score plots as a function of time for PC1. (B) PCA score plots as a function of time for PC2. (C) Average tomato leaf spectra for each time point of analysis; arrows indicate bands mainly represented in PC1, mostly correlated with time. (D) Average tomato leaf spectra of all mock and all TSWV-infected plants; arrows indicate bands mainly represented in PC2, mostly correlated with TSWV infection, with a magnification of the Raman spectral regions with major differences between control samples (Mock) and TSWV.

Therefore, the variations induced by TSWV are masked by changes liked to plant ageing arising from the same spectral bands, supporting the concept that TSWV provokes premature ageing signals. In particular, based on the model loadings and the percent of variance captured by each PC (Figure S2), TSWV induced a general decrease of the entire spectrum intensity (Figure 4C), accompanied by rising of the low-intensity peaks at 1468, 1424, 1396, and 1242 cm^{-1} (Figure 4D). Small, but statistically significant differences between mock-inoculated and TSWV-infected plants were also revealed for bands at 1072, 1020, 1013, and 974 cm^{-1} (Figure 4D).

Interestingly, when we analyzed plants in the first week after TSWV inoculation (short-term experiment), similar conclusions were reached. Here, the PCA model calculated with spectra collected at 2, 5 and 8 dpi highlighted non-random variations due to TSWV infection. Most

information was captured by the first two components that correlated with virus infection (PC1) and plant ageing (PC2) (Figure 5 A, B).

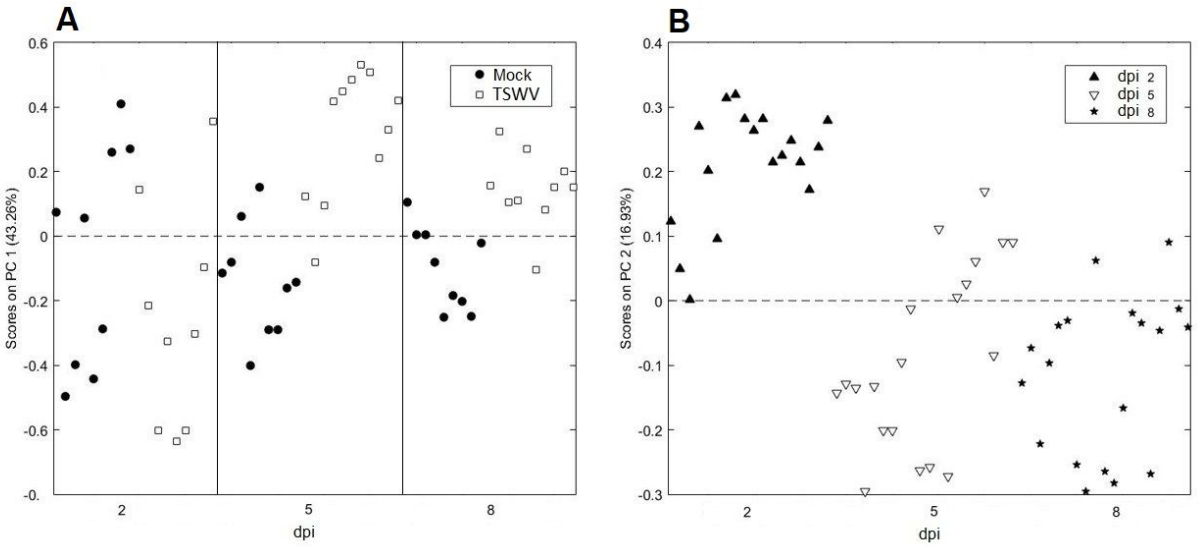

Figure 5: PCA scores plots of TSWV early-infected plants. (A) Scores of PC1 plotted against dpi and colored by infection conditions. (B) Scores of PC2 plotted against dpi and colored by time of analysis.

Therefore, in this case, the spectral changes due to virus infection prevail compared to the ageing effects occurring during one week. In particular, infected samples showed on average higher scores on PC1, already since 5 dpi, whereas the scores on PC2 gradually decreased from 2 to 5 dpi, confirming that PC2 captures information related to plant aging. The loadings of PC1 and PC2 of the model calculated for this short-term experiment exhibit several bands responsible for the differences between healthy and infected samples, but the most relevant variance was associated with the carotenoid peak at 1526 cm^{-1}, that relatively decreased in virus infected samples (Figure S3).

Supervised data analysis of Raman spectra during virus infection. To gather indications about the sensitivity, specificity and accuracy of RS in the identification of infected plants, PLS-DA classification models were calculated. These results were validated by the "leave-one group-out" cross-validation using one plant at a time as cancellation group, the most robust procedure when a separate external validation set is not available. For both viruses, an increasing trend of all figures of merit along the time frame considered (Table 2) was obtained, showing that mock-inoculated and experimentally infected samples can be distinguished with >70% accuracy since 14 dpi for TYLCSV. Moreover, RS provided positive results also for the very early detection of TSWV, i.e. within the first 8 dpi, with an accuracy >85%. Therefore, RS allowed to recognize infected plants since the early stages of infection, when symptoms are visually undetectable.

Table 2. Identification of virus infection by PLS-DA classification in "leave-one-plant-out" cross-validation.

Virus	dpi	Sensitivity	Specificity	Accuracy	Class. Error %
TYLCSV	7	0.71	0.64	0.67	33
	14	0.80	0.67	0.71	29
	21	0.78	0.78	0.78	22
	28	0.80	0.88	0.83	17
TSWV	2	0.67	0.33	0.50	50
	5	0.91	0.56	0.75	25
	8	0.80	1.00	0.89	11
	14	0.67	1.00	0.87	13
	21	0.78	1.00	0.90	10
	28	0.67	1.00	0.83	17

When comparing the loadings of the above models for TYLCSV and TSWV, differences in the relevant spectral regions for virus detection were revealed, suggesting that different viruses provoke specific modifications. To confirm this evidence and possibly distinguish the effect of the two viruses, a PLS-DA model was calculated to classify TYLCSV- vs. TSWV-infected samples. To highlight differences specifically due to each virus, independently from plant ageing, all the spectra of infected plants at the different time points were used as training set. Noteworthy, we detected a remarkable class separation between TYLCSV- and TSWV-infected plants (Figure 6) with three latent variables (LVs) (the loadings of the considered LVs are shown in Figure S4).

Table 3. Virus discrimination (TYLCSV vs. TSWV) by PLS-DA classification in "leave-one-plant-out" cross-validation (CV). The first two lines represent the confusion matrix in CV.

	Pred. TSWV	Pred. TYLCSV
True TSWV	25	8
True TYLCSV	8	27
Sensitivity	0.76	0.77
Specificity	0.77	0.76
Accuracy	0.76	0.76
Class. error %	24	24

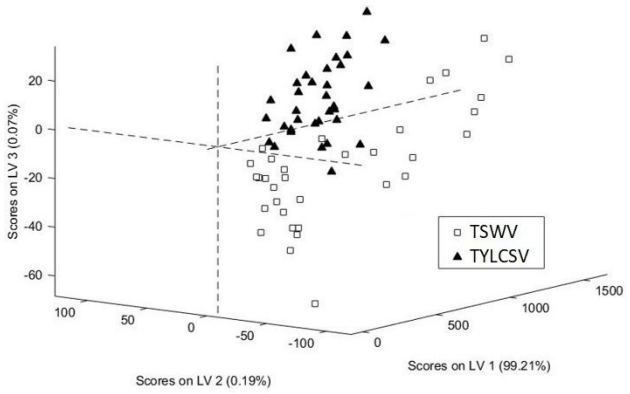

Figure 6: Classification model for the discrimination of TYLCSV vs. TSWV in tomato plants. LS-DA scores on the first three of the model.

Moreover, the "leave-one plant-out" cross-validation indicated that sensitivity, specificity and accuracy values were > 75% (Table 3), confirming that specific spectral features can be associated to each virus, according to the previous unsupervised data elaboration. This result could be linked to

the different nature of the two viruses, TSWV infecting all plant tissues and rapidly invading the plant, TYLCSV restricted to few phloem cells and slowly colonizing the plant [45].

CONCLUSIONS

The current research contributes to develop alternative, automated and non-destructive technologies for plant disease and stress evaluation, helpful to reach objective, reliable and quick plant diagnostic procedures required in a new era of precision agriculture [18,27,43,46-49]. RS represents a rapid, specific and sensitive tool to realize practical and cheap methods for large-scale disease monitoring in real time, alternative to molecular and traditional techniques.

In this work, we applied for the first time RS to monitor the spectral changes occurring during virus infection of an important crop plant, in a time frame including early (asymptomatic) and late infection stages, monitoring in parallel the amount of infecting virus using quantitative molecular approaches. A coherent modification of the entire spectral profile in virus-infected plants was detected in regions associated with carotenoids, chlorophylls, carbohydrates, and phenolic compounds. The more informative spectral regions related to the early onset of virus infection were identified by PCA. Unexpectedly, such analysis also revealed differences related to plant ageing, even if samples always consisted of newly emerged leaves. Noteworthy, RS captured not only the effect of infection since early and still asymptomatic infection stages for both tested viruses, but could also differentiate TYLCSV and TSWV, identifying relevant and specific spectral variations between them.

Conclusively, RS could be applied in plant breeding programs for disease resistance monitoring, under phytosanitary surveillance screenings, particularly relevant for the viruses here considered for which the most effective control strategies rely on selection of resistant genotypes [6,50]. Nonetheless, this study provides interesting clues to screen other species of interest exposed to different biotic or abiotic stimuli.

ORCID

Luisa Mandrile	0000-0002-5597-2590
Laura Miozzi	0000-0003-0410-8230
Anna Maria Vaira	0000-0001-6702-1162
Andrea M. Giovannozzi	0000-0001-6646-5052
Andrea M. Rossi	0000-0001-5638-7978
Emanuela Noris	0000-0001-8656-8841

Author Contributions

EN, LMandrile, LMiozzi, and AMR designed the experiments; LMandrile, SR, EN performed the experiments; LMandrile, LMiozzi, SR, AMV, AMG, AMR analyzed the data, EN and LMandrile wrote the manuscript. All authors approved the final version of the manuscript.

Notes

The authors declare no competing financial interest.

ACKNOWLEDGEMENTS. The authors thank Daniele Marian for plant care assistance. This work was supported by Progetto IMPreSA (POR FESR 2014/20 - Asse I, Azione I.1.a.1.5 INFRA-P Sostegno alle infrastrutture di ricerca considerate critiche/cruciali per i sistemi regionali) from Regione Piemonte.

References

(1) Alexandratos, N.; Bruinsma, J., World agriculture towards 2030/2050: the 2012 revision; ESA Working paper FAO, Rome2012.
(2) Bergougnoux, V. *Biotechnol Adv* **2014**, *32*, 170-189.
(3) Scholthof, K. B.; Adkins, S.; Czosnek, H.; Palukaitis, P.; Jacquot, E.; Hohn, T.; Hohn, B.; Saunders, K.; Candresse, T.; Ahlquist, P.; Hemenway, C.; Foster, G. D. *Mol Plant Pathol* **2011**, *12*, 938-954.
(4) Moyer, J. W. *Tospoviruses(Bunyaviridae)*; Academic Press: San Diego, CA, 1999.
(5) Pappu, H. R.; Jones, R. A.; Jain, R. K. *Virus Res* **2009**, *141*, 219-236.
(6) Oliver, J. E.; Whitfield, A. E. *Annu Rev Virol* **2016**, *3*, 101-124.
(7) Goldbach, R.; Peters, D. *Seminars in Virology* **1994**, *5*, 8.
(8) Adkins, S. *Molecular Plant Pathology* **2000**, *1*, 151-157.
(9) Rojas, M. R.; Macedo, M. A.; Maliano, M. R.; Soto-Aguilar, M.; Souza, J. O.; Briddon, R. W.; Kenyon, L.; Rivera Bustamante, R. F.; Zerbini, F. M.; Adkins, S.; Legg, J. P.; Kvarnheden, A.; Wintermantel, W. M.; Sudarshana, M. R.; Peterschmitt, M.; Lapidot, M.; Martin, D. P.; Moriones, E.; Inoue-Nagata, A. K.; Gilbertson, R. L. *Annu Rev Phytopathol* **2018**, *56*, 637-677.
(10) Caciagli, P.; Bosco, D. *Phytopathology* **1997**, *87*, 610-613.
(11) Turina, M.; Tavella, L.; Ciuffo, M. *Adv Virus Res* **2012**, *84*, 403-437.
(12) Nicolaisen, M. *J Virol Methods* **2011**, *173*, 137-143.
(13) Boonham, N.; Smith, P.; Walsh, K.; Tame, J.; Morris, J.; Spence, N.; Bennison, J.; Barker, I. *J Virol Methods* **2002**, *101*, 37-48.
(14) Accotto, G. P.; Navas-Castillo, J.; Noris, E.; Moriones, E.; Louro, D. *European Journal of Plant Pathology* **2000**, *106*, 179-186.
(15) Accotto, G. P.; Noris, E.; Czosnek, H. *Detection methods for TYLCV and TYLCSV*, 2007, p 241-249.
(16) Mason, G.; Caciagli, P.; Accotto, G. P.; Noris, E. *J Virol Methods* **2008**, *147*, 282-289.
(17) Noris, E.; Miozzi, L. *Methods Mol Biol* **2015**, *1236*, 61-72.
(18) Khaled, A. Y.; Abd Aziz, S.; Bejo, S. K.; Nawi, N. M.; Seman, I. A.; Onwude, D. I. *Applied Spectroscopy Reviews* **2018**, *53*, 36-64.
(19) Mandrile, L.; Fusaro, I.; Amato, G.; Marchis, D.; Martra, G.; Rossi, A. M. *Food Chem* **2018**, *267*, 240-245.
(20) Naumann, D. *Applied Spectroscopy Reviews* **2001**, *36*, 239-298.
(21) Mandrile, L.; Amato, G.; Marchis, D.; Martra, G.; Rossi, A. M. *Food Chem* **2017**, *229*, 268-275.
(22) Mandrile, L.; Giovannozzi, A. M.; Durbiano, F.; Martra, G.; Rossi, A. M. *Food Chem* **2018**, *244*, 16-24.
(23) Mandrile, L.; Zeppa, G.; Giovannozzi, A. M.; Rossi, A. M. *Food Chem* **2016**, *211*, 260-267.
(24) Rys, M.; Juhász, C.; Surówka, E.; Janeczko, A.; Saja, D.; Tóbiás, I.; Skoczowski, A.; Barna, B.; Gullner, G. *Plant Physiol Biochem* **2014**, *83*, 267-278.

(25) Yeturu, S.; Vargas Jentzsch, P.; Ciobotă, V.; Guerrero, R.; Garrido, P.; Ramos, L. A. *Analytical Methods* **2016**, *8*, 3450-3457.
(26) Pérez, M. R.; Mendoza, M. G.; Elías, M. G.; González, F. J.; Contreras, H. R.; Servín, C. C. *Appl Spectrosc* **2016**, *70*, 829-839.
(27) Farber, C.; Kurouski, D. *Anal Chem* **2018**, *90*, 3009-3012.
(28) Wold, S.; Esbensen, K.; Geladi, P. *Chemometrics and Intelligent Laboratory Systems* **1987**, *2*, 37 - 52.
(29) Barker, M.; Rayens, W. *Journal of Chemometrics* **2003**, *17*, 166-173.
(30) Barnes, R. J.; Dhanoa, M. S.; Lister, S. J. *Applied Spectroscopy* **1989**, *43*, 772-777.
(31) Catoni, M.; Miozzi, L.; Fiorilli, V.; Lanfranco, L.; Accotto, G. P. *Mol Plant Microbe Interact* **2009**, *22*, 1504-1513.
(32) Vítek, P.; Jehlička, J.; Edwards, H. G.; Osterrothová, K. *Analytical and bioanalytical chemistry* **2009**, *393*, 1967-1975.
(33) Schulz, H.; Baranska, M.; Baranski, R. *Biopolymers* **2005**, *77*, 212-221.
(34) Schlücker, S.; Szeghalmi, A.; Schmitt, M.; Popp, J.; Kiefer, W. *Journal of Raman Spectroscopy* **2003**, *34*, 413-419.
(35) Pudney, P. D. A.; Gambelli, L.; Gidley, M. J. *Applied Spectroscopy* **2011**, *65*, 127-134.
(36) Schrader, B.; Klump, H. H.; Schenzel, K.; Schulz, H. J. *Journal of Molecular Structure* **1999**, *509*, 201 - 212.
(37) Agarwal, U. P.; Ralph, S. A. *Applied Spectroscopy* **1997**, *51*, 1648-1655.
(38) Eravuchira, P. J.; El-Abassy, R. M.; Deshpande, S.; Matei, M. F.; Mishra, S.; Tandon, P.; Kuhnert, N.; Materny, A. *Vibrational Spectroscopy* **2012**, *61*, 10 - 16.
(39) Koyama, Y.; Umemoto, Y.; Akamatsu, A.; Uehara, K.; Tanaka, M. *Journal of Molecular Structure* **1986**, *146*, 273 - 287.
(40) Boldt, N. J.; Donohoe, R. J.; Birge, R. R.; Bocian, D. F. *Journal of the American Chemical Society* **1987**, *109*, 2284-2298.
(41) Gill, D.; Kilponen, R. G.; Rimai, L. *Nature* **1970**, *227*, 743-744.
(42) Li, Y.; Cui, H.; Cui, X.; Wang, A. *Curr Opin Virol* **2016**, *17*, 19-24.
(43) Altangerel, N.; Ariunbold, G. O.; Gorman, C.; Alkahtani, M. H.; Borrego, E. J.; Bohlmeyer, D.; Hemmer, P.; Kolomiets, M. V.; Yuan, J. S.; Scully, M. O. *Proc Natl Acad Sci U S A* **2017**, *114*, 3393-3396.
(44) Miozzi, L.; Napoli, C.; Sardo, L.; Accotto, G. *Plos One* **2014**, *9*.
(45) Morilla, G.; Krenz, B.; Jeske, H.; Bejarano, E. R.; Wege, C. *J Virol* **2004**, *78*, 10715-10723.
(46) López, M. M.; Bertolini, E.; Olmos, A.; Caruso, P.; Gorris, M. T.; Llop, P.; Penyalver, R.; Cambra, M. *Int Microbiol* **2003**, *6*, 233-243.
(47) Sankaran, S.; Mishra, A.; Ehsani, R.; Davis, C. *Computers and Electronics in Agriculture* **2010**, *72*, 1 - 13.
(48) Yang, D.; Ying, Y. *Applied Spectroscopy Reviews* **2011**, *46*, 539-560.
(49) Gierlinger, N.; Keplinger, T.; Harrington, M. *Nat Protoc* **2012**, *7*, 1694-1708.
(50) Yan, Z.; Pérez-de-Castro, A.; Díez, M. J.; Hutton, S. F.; Visser, R. G. F.; Wolters, A. A.; Bai, Y.; Li, J. *Front Plant Sci* **2018**, *9*, 1198.